

# Novel Interpolation Method of Multi-DFT-Bins for Frequency Estimation of Signal with Parameter Step Change

Kai Wang, Shan Liu, Lanlan Wang, Janusz Smulko and He Wen

**Abstract**—The IpDFT(Interpolation Discrete Fourier Transform) method is one of the most commonly used non-parametric methods. However, when a parameter(frequency, amplitude or phase) step changes in the DFT period, the DFT coefficients will be distorted seriously, resulting in the large estimation error of the IpDFT method. Hence, it is a key challenge to find an IpDFT method, which not only can eliminate the effect of the step-changed symbol, but also can sufficiently eliminate the fence effect and the spectrum leakage. In this paper, an IpDFT based method is proposed to estimate the frequency of the single tone signal with the step-changed parameters in the sampling signal sequence. The relationship between the DFT bins and the step changed parameters is given by several linear equations. At most six different DFT bins are used to eliminate the effect of symbol.

**Index Terms**—Interpolation Discrete Fourier Transform (DFT); frequency estimation; the single tone signal; step-changed parameter; RF conformance test.

## I. INTRODUCTION

WITH the development of signal processing technology, frequency estimation plays an increasingly important role in this field. A large number of parametric methods (time-domain methods) the non-parametric methods (frequency-domain methods) have emerged in the past few decades. For example, the ML (Maximum likelihood) method [1], [2], the Wavelet method [3], the filtering method [4], [5], PLL (Phase locked loop) method [6], prony method [7], Taylor Fourier Filter method [8], [9] and the IpDFT method (the interpolation Discrete Fourier Transform).

The IpDFT method and its improvements, such as the e-IpDFT [10] and i-IpDFT [11], which can be simplified by the Fast Fourier Transform (FFT), is currently one kind of the most commonly used non-parametric methods [12], [13]. The DFT-based estimators are fast and very simple to apply [14], [15]. For the single tone signal, the IpDFT methods have completely solved the estimation error caused by the fence effect.

This work was supported in part by the National Key Research and Development Program of China under Grant 2020YFC2004003 and Grant 2020YFC2004002, the National Natural Science Foundation of China under Grant 61771190 and in part by the Natural Science Foundation of Hunan Province under Grant 2019JJ20001.

Kai Wang, Shan Liu and Lanlan Wang are with the School of Information Science and Engineering, Southeast University, 9 Mozhoudonglu, Jiangning District, Nanjing 211111, China(e-mail: kaiwang@seu.edu.cn; Jasmine\_63@163.com; wanglanlan\_12138@163.com).

Janusz Smulko is with Gdansk University of Technology, Poland

He Wen is with the College of Electrical and Information Engineering, Hunan University, Changsha, Hunan Province(e-mail: he\_wen82@126.com)

With two or three DFT bins, various IpDFT methods [16]–[18] are proposed to estimate the frequency of the signal. For the real-value harmonic signal, the most important challenge is how to compensate for spectrum leakages, which heavily damages the estimation accuracy [19]–[22]. Many variants of DFT, such as Sliding DFT [23], Taylor Fourier Filter method [8], [9], Iterative IpDFT [24] and Frequency Shifting Filtering [25], have been reported to estimate the phasor parameters. All of these methods try to compensate for spectrum leakages, which are caused by the off-nominal frequency operation of the system.

In the IpDFT method, windowing techniques such as the maximum decay sidelobe window [26], [27] and the triangular self-convolution window [28] are also used to reduce harmonic and inter-harmonic interference. Besides windowing techniques, another method is to consider the contribution of each frequency component in the spectrum and to solve the spectrum leakage problem theoretically. [29], [30] completely eliminate the influence of spectrum leakage by a three-point IpDFT based on MDW. Furthermore, the authors of [30] apply the algorithm of [29] to the harmonic signal. Other authors [31], [32] propose an IpDFT based on a scaling factor to estimate the dominant chatter frequency. Based on the rectangular window, [33]–[35] introduce an efficient two-point/three-point IpDFT of the sinusoid signal with or without the damping factor. [36], [37] combine the CLS (complex-value least squares) criteria and SDFT (Smart DFT) to obtain higher algorithm accuracy.

The default signal model in IpDFT methods is the time invariant signal, which means the amplitude, phase and frequency of the signal remain unchanged during the sampling period. However, the time-varying signals also have research significance in real-world scenarios. For example, the basic of RF conformance testing system is a fast and accurate frequency offset estimation method for the wireless systems with different modulation signals, such as quadrature amplitude modulation signal (QAM), phase-shift keying signal (PSK) and frequency-shift keying signal (FSK) [38], [39]. QAM signal, PSK signal and FSK signal can be regarded as carrier signals whose amplitude, phase and frequency vary with the transmission information during different sampling cycles [40], [41]. In the power systems, the precise and rapid frequency estimation is also necessary in PMUs (phasor measurement units) [42], [43]. The standards of phasors estimation provide detailed test requirements for the time-varying signal, including step change in amplitude, phase and frequency

[44]–[46]. However, the research of IpDFT based frequency estimation for the time-varying signal frequency estimation is still in the preliminary stage. Others [47] propose a low complexity IpDFT method to estimate frequency offset for M-QAM coherent optical systems. A novel IpDFT frequency estimation method of single tone signal with bit transition is proposed in [48].

The signals with step-changed parameters are the most important and basic signal modes in the wireless system [40], [41] or the power system [44]–[46]. The basic algorithms, which are utilized in the RF conformance test [38], [39] or in the phasor measurement units [42], [43], are also used for the frequency estimation in different signal modes. A rapid and accurate estimation can greatly ensure reliable performance of the test system. However, when a parameter step changes in the DFT period, the DFT coefficients will be distorted seriously, resulting in the large estimation error of the IpDFT method. Hence, it is a key challenge to find an IpDFT method, which not only can eliminate the effect of the step-changed symbol, but also can sufficiently eliminate the fence effect and the spectrum leakage. In this paper, an IpDFT based method is proposed to estimate the frequency of the single tone signal with the step-changed parameter in the sampling signal sequence. The relationship between the DFT bins and the step-changed parameters is given by several linear equations. At most six different DFT bins are used to eliminate the effect of the step-changed parameters. The results of simulation and experiment confirm that the proposed algorithm can achieve frequency estimation with high accuracy.

## II. FREQUENCY ESTIMATION METHOD

A single tone signal with the step-changed parameters can be described as

$$\begin{aligned} x(n) &= s(n) + q(n) \\ &= A_m \exp(\varphi_m) \exp(j\omega_m n) + q(n) \end{aligned} \quad (1)$$

where  $A_m$ ,  $\varphi_m$  and  $\omega_m = 2\pi f_m T_s$  are the  $m$ -th ( $m \in [0, M - 1]$ ) unknown parameters of the amplitude, the phase and the angular frequency.  $q(n)$  is the additive white Gaussian noise (AWGN) with variance  $\sigma_q^2$ .  $f_m$  is the signal frequency and  $T_s$  is the sampling time.

When we obtain an  $N$ -sample time sequence  $x(n)$ , we rewrite the symbols of the  $m$ -th jump as  $U_m$  and  $\omega_m$  where  $\omega_m = 2\pi l_m / N = 2\pi(k_m + \delta_m) / N$ ,  $l_m$  is the  $m$ -th acquired signal cycles.  $\delta_m \in [-0.5, 0.5]$  and  $k_m \in [0, 1, \dots, \frac{N}{2} - 1]$  are the fractional-part and the integer-part of  $l_m$ . The  $N$ -point DFT of  $x(n)$  is:

$$\begin{aligned} X(k) &= \sum_{n=0}^{N-1} s(n) W_N^{nk} + \sum_{n=0}^{N-1} q(n) W_N^{nk} \\ &= S(k) + Q(k) \end{aligned} \quad (2)$$

where  $W_N^k = e^{-j(\frac{2\pi}{N})k}$ ,  $S(k)$  and  $Q(k)$  are the DFTs of  $s(n)$  and  $q(n)$ .

*A. the case when the frequency, the amplitude and the phase all step change*

In this part, we only consider the case of one step-change in an  $N$ -length signal. Let the parameters (frequency, amplitude or phase) step change on the  $L$ -th sample. The angular frequency before the step-change is denoted as  $\omega_1$  and the angular frequency after the step-change is denoted as  $\omega_2$ :

$$s(n) = \begin{cases} U_1 e^{j\omega_1 n}, & n = 0, 1, \dots, L-1 \\ U_2 e^{j\omega_2 n}, & n = L+1, L+2, \dots, N-1 \end{cases} \quad (3)$$

where  $U_1 = A_1 \exp(\varphi_1)$  and  $U_2 = A_2 \exp(\varphi_2)$  are any two different unknown parameters of amplitude and phase combination. The DFT result at slot  $k$  changes to:

$$\begin{aligned} S(k) &= \sum_{n=0}^{L-1} A_1 e^{j\varphi_1} e^{j\omega_1 n} W_N^{nk} + \sum_{n=L}^{N-1} A_2 e^{j\varphi_2} e^{j\omega_2 n} W_N^{nk} \\ &= A_1 e^{j\varphi_1} \frac{1 - (e^{j\omega_1} W_N^k)^L}{1 - e^{j\omega_1} W_N^k} + A_2 e^{j(\varphi_2 + L\omega_2)} W_N^{kL} \frac{1 - (e^{j\omega_2} W_N^k)^{N-L}}{1 - e^{j\omega_2} W_N^k} \\ &= A_1 e^{j\varphi_1} \frac{1 - (e^{j\omega_1} W_N^k)^L}{1 - e^{j\omega_1} W_N^k} + A_2 e^{j\varphi_2'} W_N^{kL} \frac{1 - (e^{j\omega_2} W_N^k)^{N-L}}{1 - e^{j\omega_2} W_N^k} \\ &= \frac{(p_1 + p_2) + (q_1 + q_2) W_N^k + (u_1 + u_2) W_N^{kL} + (v_1 + v_2) W_N^{k(L+1)}}{1 - (\lambda_1 + \lambda_2) W_N^k + \lambda_1 \lambda_2 W_N^{2k}} \end{aligned} \quad (4)$$

where  $\lambda_1 = e^{j\omega_1}$ ,  $\lambda_2 = e^{j\omega_2}$ ,  $p_1 = A_1 e^{j\varphi_1}$ ,  $p_2 = -A_2 e^{j\varphi_2'} e^{j\omega_2 L}$ ,  $q_1 = -A_1 e^{j\varphi_1} e^{j\omega_2}$ ,  $q_2 = A_2 e^{j\varphi_2'} e^{j(\omega_1 + \omega_2)(N-L)}$ ,  $u_1 = -A_1 e^{j\varphi_1} e^{j\omega_1 L}$ ,  $u_2 = A_2 e^{j\varphi_2'}$ ,  $v_1 = A_1 e^{j\varphi_1} e^{j(\omega_2 + \omega_1 L)}$ ,  $v_2 = -A_2 e^{j\varphi_2'} e^{j\omega_1}$  and  $\varphi_2' = \varphi_2 + L\omega_2$ . The coarse frequency estimation can be performed as:  $\hat{k}_0 = \arg \max_{k \in \{0, 1, \dots, N-1\}} (|X(k)|)$ . When we get any six different DFT bins  $\mathbf{X}(k) = [X(k_1), X(k_2), \dots, X(k_6)]^T$ , we can get the following linear equations according to (4):

$$\mathbf{X}_k = \mathbf{W}_k \boldsymbol{\eta} \quad (5)$$

where  $\boldsymbol{\eta}$  and  $\mathbf{W}_k$  can be written as:

$$\boldsymbol{\eta} = [p_1 + p_2, q_1 + q_2, u_1 + u_2, v_1 + v_2, \lambda_1 + \lambda_2, \lambda_1 \lambda_2]^T \quad (6)$$

$$\mathbf{W}_k = \begin{bmatrix} 1 & W_N^{k_1} & W_N^{k_1 L} & W_N^{k_1(L+1)} & X(k_1) W_N^{k_1} & -X(k_1) W_N^{2k_1} \\ 1 & W_N^{k_2} & W_N^{k_2 L} & W_N^{k_2(L+1)} & X(k_2) W_N^{k_2} & -X(k_2) W_N^{2k_2} \\ 1 & W_N^{k_3} & W_N^{k_3 L} & W_N^{k_3(L+1)} & X(k_3) W_N^{k_3} & -X(k_3) W_N^{2k_3} \\ 1 & W_N^{k_4} & W_N^{k_4 L} & W_N^{k_4(L+1)} & X(k_4) W_N^{k_4} & -X(k_4) W_N^{2k_4} \\ 1 & W_N^{k_5} & W_N^{k_5 L} & W_N^{k_5(L+1)} & X(k_5) W_N^{k_5} & -X(k_5) W_N^{2k_5} \\ 1 & W_N^{k_6} & W_N^{k_6 L} & W_N^{k_6(L+1)} & X(k_6) W_N^{k_6} & -X(k_6) W_N^{2k_6} \end{bmatrix} \quad (7)$$

According to Eq.(5),  $\boldsymbol{\eta}$  can be estimated as:

$$\hat{\boldsymbol{\eta}} = \mathbf{W}_k^{-1} \mathbf{X}_k \quad (8)$$

where  $\hat{\cdot}$  is the estimated value of ( $\cdot$ ). Let  $\hat{\lambda}_1 + \hat{\lambda}_2 = a$  and  $\hat{\lambda}_1 \hat{\lambda}_2 = b$ , where  $a$  and  $b$  are calculated from Eq. (6).  $\omega_1$  and

149  $\omega_2$  can be estimated as:

$$\begin{cases} \hat{\omega}_1 = \frac{\text{Im}(\ln(a + \sqrt{a^2 - 4b}))}{2} \\ \hat{\omega}_2 = \frac{\text{Im}(\ln(a - \sqrt{a^2 - 4b}))}{2} \end{cases} \quad (9)$$

150  
151 Although any of the six different DFT bins can be used in  
152 our method, it is recommended to use the DFT bins with the  
153 six largest magnitudes to obtain the best estimation results in  
154 practical applications.

155 *B. the case when the amplitude and the phase step change,*  
156 *but the frequency keeps unchange*

157 In this part, we keep the frequency constant, and let the  
158 amplitude and the phase step change during the sampling  
159 signal sequence. In order to distinguish the frequency step  
160 change of part A,  $\omega_0$  is chosen to represent the signal angular  
161 frequency. Eq.(4) can be simplified as:

$$\begin{aligned} S(k) &= \sum_{n=0}^{L-1} A_1 e^{j\varphi_1} e^{j\omega_0 n} W_N^{nk} + \sum_{n=L}^{N-1} A_2 e^{j\varphi_2} e^{j\omega_0 n} W_N^{nk} \\ &= A_1 e^{j\varphi_1} \frac{1 - (e^{j\omega_0} W_N^k)^L}{1 - e^{j\omega_0} W_N^k} + A_2 e^{j\varphi_2} W_N^{kL} \frac{1 - (e^{j\omega_0} W_N^k)^{N-L}}{1 - e^{j\omega_0} W_N^k} \quad (10) \\ &= \frac{(\mu_1 - v_2) + (\mu_2 - v_1) W_N^{kL}}{1 - \lambda_0 W_N^k} \end{aligned}$$

162 where  $\mu_1 = A_1 e^{j\varphi_1}$ ,  $\mu_2 = A_2 e^{j\varphi_2}$ ,  $v_1 = A_1 e^{j\varphi_1} (\lambda_0)^L$ ,  
163  $v_2 = A_2 e^{j\varphi_2} (\lambda_0)^{N-L}$  and  $\lambda_0 = e^{j\omega_0}$ . When we get any  
164 three different DFT bins  $\mathbf{X}_k = [X(k_1), X(k_2), X(k_3)]^T$ ,  $\eta =$   
165  $[\mu_1 - v_2, \mu_2 - v_1, \lambda_0]^T$  can be estimated as:

$$\hat{\eta} = \mathbf{W}_k^{-1} \mathbf{X}_k \quad (11)$$

166 where

$$\mathbf{W}_k = \begin{bmatrix} 1 & W_N^{k_1 L} & X(k_1) W_N^{k_1} \\ 1 & W_N^{k_2 L} & X(k_2) W_N^{k_2} \\ 1 & W_N^{k_3 L} & X(k_3) W_N^{k_3} \end{bmatrix} \quad (12)$$

167  $\omega_0$  can be estimated as:

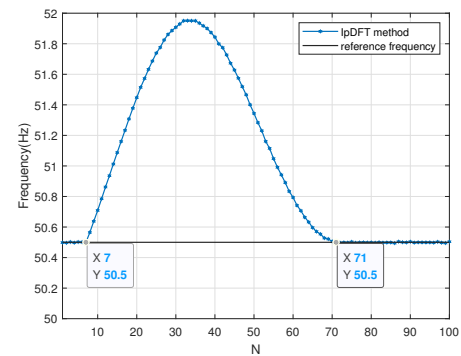
$$\hat{\omega}_0 = \text{Im}(\ln \hat{\lambda}_0) \quad (13)$$

169 In this condition, the DFT bin with the largest magnitude  
170 and its adjacent DFT bins:  $X(k_0)$ ,  $X(k_0 + 1)$ ,  $X(k_0 - 1)$  are  
171 recommended in practical applications for better estimation  
172 results.

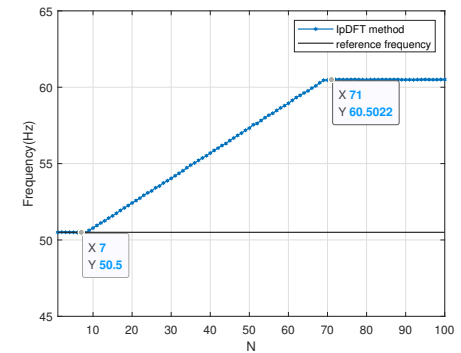
173 *C. Estimation Method of the location of bit transition L*

174 The actual location of bit transition  $L$  is important in the  
175 proposed algorithm according to Eq. (4) and Eq. (10). In the  
176 calculation process, if the value of  $L$  is wrong, it will cause  
177 the frequency estimation error. In Refs. [47], [48],  $L$  is set to a  
178 known value by default. However, it is not always an easy job  
179 because it is simply impossible to know the transition time  
180 beforehand in any measurement. If  $L$  is unknown, we can  
181 use a sliding window based time-frequency estimation to get

182 the value of  $L$ . Assuming the signal of length  $N = 128$ , the  
183 step-change of parameter occurs at an unknown point  $L$ . We  
184 choose a rectangular window with a window size of  $N' = 64$   
185 and a step length of 1. By using this rectangular window, we  
186 divide the signal into 65 data frames. The frame length and the  
187 frame shift of each data frame are 64 and 1, respectively. For  
188 the any  $m$ -th data frame:  $\{x(m - 63), x(m - 1), \dots, x(m)\}$ , the  
189 IpDFT method given in [16] is used to estimate the  
190 frequency  $\omega(m)$  of the  $m$ -th data frame. The estimation results  
191 for the step-changed signals when SNR=40dB are shown in  
192 Figure 1. As shown in Fig. 1(a), the amplitude and the phase  
193 jump point appears at 7-th point and 71-st point, which means  
194 the location of bit transition  $L$  is 7. We can also use  $71-64=7$   
195 to obtain the same result. As shown in Fig. 1(b), the frequency  
196 jump point appears at the point as same as the Fig. 1(a) and  
197 it obtains the same result.



(a)



(b)

Fig. 1: The sliding window based time-frequency estimation (a) the step-change of the amplitude and the phase; (b) the step-change of the frequency

198 The sliding window method can be utilized as a  
199 coarse estimation of the location  $L$ . Furthermore, we  
200 will analyze the effect of transition time error in the  
201 frequency estimation and discuss its impact in this paper.  
202 We denote the estimated location by the coarse estimation  
203 as  $L'$  and then we can get a set  $L$  consisting of  $L'$  and  
204 its neighbors:  $L = \{\dots, L' - 2, L' - 1, L', L' + 1, L' + 2, \dots\}$ .  
205 With the elements in set  $L$  in turn, we estimate  
206  $\omega$  according to the method proposed in section  
207 II and denote the estimated values as:  $\omega(L) =$

TABLE I: MSEs of  $\hat{\omega}$  with different sampling points in different conditions(unit: dB)

L	60	61	62	63	64	65	66	67	68	69	70
<b>Condition: the step-change of the amplitude and the phase</b>											
noiseless	-68.6849	-74.9372	-85.5932	-101.7746	-320.2516	-82.0556	-72.7839	-66.9066	-62.5740	-59.1483	-56.3269
SNR=40dB	-68.5969	-74.9061	-83.1398	-85.5546	-86.8574	-80.4095	-72.7481	-66.9098	-62.5128	-59.1237	-56.3227
SNR=15dB	-61.1405	-61.2445	-62.1591	-61.3460	-60.5947	-61.1215	-61.2578	-60.4537	-59.6906	-57.9072	-54.7129
<b>Condition: the step-change of the frequency</b>											
noiseless	-37.6932	-40.5259	-44.3341	-50.5133	-254.3888	-50.1606	-43.4749	-38.9035	-35.0644	-31.6950	-28.7563
SNR=40dB	-37.6995	-40.5325	-44.3040	-50.5135	-76.8406	-50.1302	-43.4625	-38.9028	-35.0705	-31.6894	-28.7464
SNR=15dB	-36.9852	-38.0281	-42.3912	-40.3862	-41.1338	-44.3340	-42.7269	-38.7947	-34.9241	-31.823	-28.7188

208  $\{\dots, \omega(L' - 2), \omega(L' - 1), \omega(L'), \omega(L' + 1), \omega(L' + 2), \dots\}$ .  
 209 In Tab. I, we calculate the MSEs (The mean square error)  
 210 between the actual frequency of signal  $\omega$  and the estimated  
 211 frequencies with different location  $\omega(L)$  in noiseless/ noisy  
 212 condition.

213 There are two factors that affect the estimation accuracy of  
 214 our method. One is the value of SNR. The other is the value  
 215 of  $L'$ . In the low noise environment, the influence of the value  
 216 of  $L'$  is more important. As shown in Tab. I, we can accurately  
 217 estimate  $\omega$  when the value of  $L'$  is right( $L' = L$ ) When the  
 218 value of  $L'$  is wrong( $L' \neq L$ ), our method is a biased estimation  
 219 algorithm. The estimation error will gradually increase with  
 220 the increasing of the difference between  $L$  and  $L'$ . In the high-  
 221 noise environment, the influence of SNR is more important.  
 222 The influence of the error  $L'$ , whose value is slightly different  
 223 from the real value  $L$ , can be ignored in the estimation process.  
 224 We can get the estimated values with little differences even we  
 225 use the wrong  $L'$  when SNR=15dB.

226 Furthermore, we calculate the differences between two  
 227 adjacent estimated frequencies according to Eq. (14). The  
 228 results in the noiseless and the low noise condition are shown  
 229 in Figure 2 and Figure 3. We set  $L = 64$ ,  $N = 128$   
 230 and  $L = \{60, 61, 62, 63, 64, 65, 66, 67, 68, 69, 70\}$ . As shown in  
 231 Fig.2, when the value of  $L'$  is equal to the actual value  $L$  the  
 232 difference between  $\omega(L)$  and adjacent estimated frequencies  
 233  $\omega(L - 1)$  is the maximum.

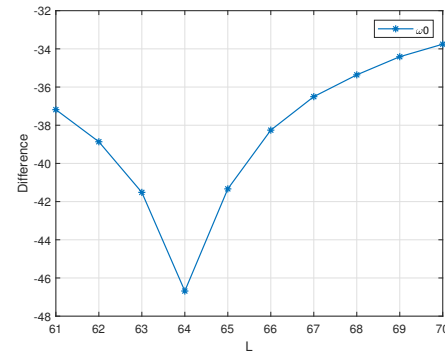
$$\text{diff}(i) = 10\log_{10} |\omega(i) - \omega(i - 1)| (i \in L) \quad (14)$$

234 In this paper, our main research purpose is to reveal the  
 235 relation between the DFT bins and the system parameters of  
 236 the signal with step-changed parameters, which allows us to  
 237 better understand the essence of discrete Fourier transform.  
 238 The research on the estimation of the location  $L$  is only at  
 239 early stage. So far, we haven't given the explicit expression  
 240 between the DFT bins and the location  $L$  in this paper. In our  
 241 future work, we will focus on this issue for further research  
 242 and discussion.

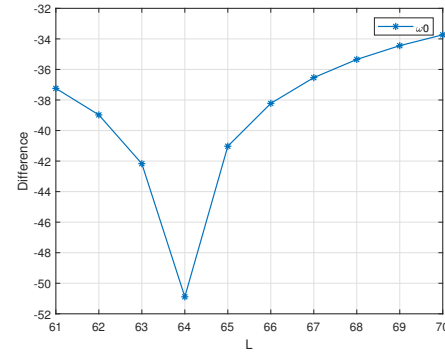
### III. PERFORMANCE OF PROPOSED METHOD

243 In this section, we focused on analyzing the estimation per-  
 244 formance of the algorithm without any practical application.  
 245 The normalized angular frequency  $\omega_i$  is chosen in this part,  
 246 where  $\omega_i = 2\pi l_i / N = 2\pi f_i / f_s$  ( $i = 0, 1$  or  $2$ ).

247 We compare the estimated performance of the considered al-  
 248 gorithm through simulation results. The considered algorithms  
 249 are the XJX method in Ref. [47], the UFE method in Ref. [48],  
 250 the BFEL method in Ref. [48], the ITE-FOE method in Ref.



(a)



(b)

Fig. 2: the difference between two adjacent estimated frequencies when the amplitude and the phase step change a) SNR=40dB; b) noiseless

[49], the DIFF-FOE method in Ref. [50]. Cramer-Rao lower bounds (CRLB) is shown in Eq.(14). 252 253

$$\text{CRLB}(\omega_0) \geq \frac{12\sigma^2}{A^2N(N^2 - 1)} \quad (15)$$

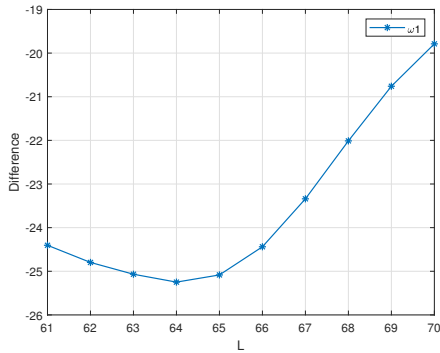
254 where  $A$  is the amplitude of the signal,  $N$  is the signal length  
 255 and  $\sigma^2$  is the variance of the additive white Gaussian noise.

256 The observed sample length  $N$  is 128. For each parameter,  
 257 3000 runs are performed to evaluate the statistical properties.  
 258 The mean square error (MSE) is used to evaluate the perfor-  
 259 mance of the proposed estimator and other algorithms, which  
 260 is given by:

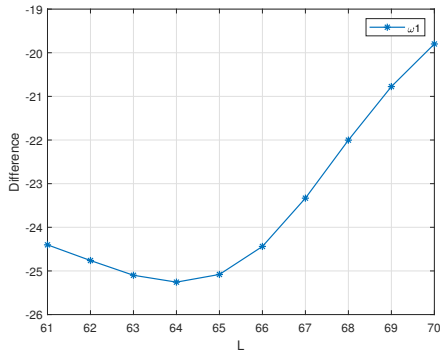
$$\text{MSE} = 10\log_{10} \left( \frac{1}{M} \sum_{i=1}^M (\hat{\omega}(i) - \omega)^2 \right) \quad (16)$$

261 where  $\hat{\omega}(i)$  presents the estimated frequency of the  $i$ -th inde-  
 262 pendent simulation.





(a)



(b)

Fig. 3: the difference between two adjacent estimated frequencies when the amplitude and the phase step change a) SNR=40dB; b) noiseless

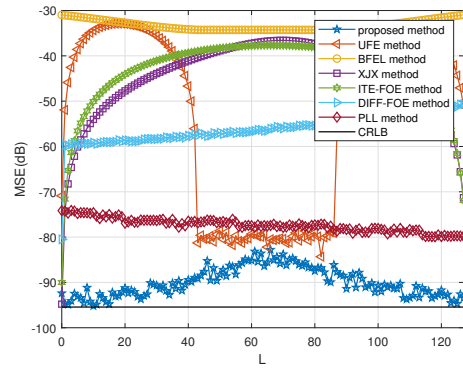


Fig. 4: MSEs of  $\hat{\omega}_0$  versus  $L$  with  $l_0=1.06$  and SNR=40dB

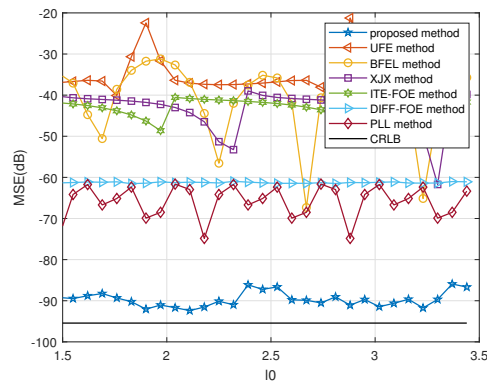


Fig. 5: MSEs of  $\hat{\omega}_0$  versus  $l_0$  with SNR=40dB and  $L=32$

263 *A. the case when the amplitude and the phase step change,*  
 264 *but the frequency keeps unchanged*

265 Firstly, let's consider the case when the amplitude and the  
 266 phase step change, but the frequency keeps unchanged. The  
 267 jumping point  $L$  of our algorithm can be applied to  $[0, N-1]$ .  
 268 When  $L = 0$  or  $N - 1$ , the signal actually degenerates into a  
 269 single-frequency complex exponential signal, and our method  
 270 actually degenerates into an IpDFT method in [16]–[18]. We  
 271 set  $U_1 = 0.9 \exp(10\pi/180)$  and  $U_2 = \exp(80\pi/180)$ . Figure 4  
 272 depicts the relationships between  $L$  and MSEs in the noisy  
 273 environment. Set  $l_0=1.06$  and let  $L$  change from 0 to 127.  
 274 As shown in Fig. 4, our method achieves better performance.  
 275 However, the UFE method only performs well when the jump  
 276 point  $L$  is in the interval  $[N/3, 2N/3]$ . Furthermore, let's  
 277 take  $L=32$  as an example to analyze the performances of our  
 278 method with different  $l_0$  or SNR.

279 Figure 5 depicts the relationships between  $l_0$  and MSEs  
 280 when SNR=40dB and  $L=32$ . Then, let  $l_0$  change from 0.5  
 281 to 3.5. As shown in Fig. 5, our method can achieve the  
 282 minimum MSE -90dB. However, the minimum MSE of UFE  
 283 is only -35dB, which means the performance of our method  
 284 is much better than that of UFE method when SNR=40dB  
 285 and  $L=32$ . Fig. 6 depicts the relationships between SNR and  
 286 MSEs when  $L=32$ . Set  $l_0=1.06$  and let SNR change from 0dB  
 287 to 40dB. The MSEs of our method decrease linearly when  
 288 SNR increases, which means that our methods can estimate

the frequency correctly when amplitude and phase step change  
 on  $L$ -th sample. However, UFE method can only estimate the  
 frequency correctly when  $L \in [N/3, 2N/3]$ . In order to verify  
 the effect of different sampling points  $N$  on the estimated  
 frequency, set  $l_0=1.06$  and SNR=40dB. The MSE of frequency  
 is shown in Table II, and the results show that our method has  
 better effect under different sampling points  $N$  when  $L=32$ .

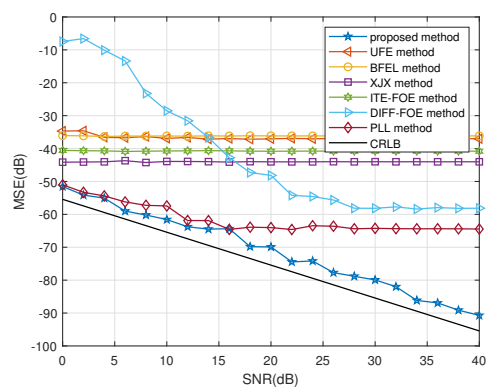


Fig. 6: MSEs of  $\hat{\omega}_0$  versus SNR with  $l_0=1.06$  and  $L=32$

Let's consider the case when the signal is distorted by the  
 DC offset or the harmonics. The signal distorted by the DC

TABLE II: MSEs of  $\hat{\omega}_0$  with different sampling points  $N$  when  $L = 32$  (unit: dB)

		Proposed Method	UFE Method	BFEL Method	XJX Method	ITE-DFT	DIFF-DFT	PLL
$L=32$	$N=128$	-83.53	-36.27	-34.19	-42.45	-39.39	-56.38	-76.34
	$N=256$	-92.98	-38.16	-38.59	-55.05	-50.63	-63.20	-81.16
	$N=512$	-101.51	-46.13	-43.72	-67.28	-62.74	-69.79	-86.23
	$N=1024$	-108.92	-56.42	-49.34	-79.42	-75.21	-76.25	-91.78

TABLE III: Condition of fundamental and harmonics

Harmonic	1st	3rd	5th	7th	9th	11th	13th	15th
Amplitude(rms)	0	-26.02	-33.97	-42.14	-53.18	-66.22	-78.26	-90.30

offset can be expressed as:

$$x(n) = s(n) + q(n) \quad (17)$$

$$= A_m \exp(\varphi_m) \exp(j\omega_m n) + A_{dc} + q(n)$$

where  $A_{dc} = 1$ . Let  $X_{dc}(k)$  be the DFT of the signal  $A_{dc}$ . When  $k > 0$ , the value of  $X_{dc}(k) = 0$ . In practical applications, if we do not use  $X_{dc}(0)$  in estimation process, we can reduce the DC offset interference. The performances distorted by the DC offset are shown in Fig. 7. Set  $L=32$  and  $SNR = 40$ dB. Our method can correctly estimate the frequencies no matter the DC offset distorted or not.

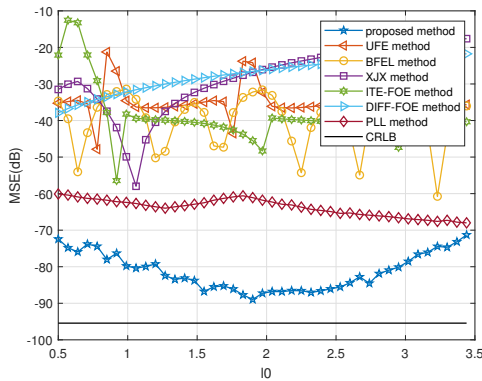


Fig. 7: MSEs of  $\hat{\omega}_0$  versus  $l_0$  with  $SNR=40$ dB,  $A_{dc} = 1$  and  $L=32$

The signal distorted by noise and the 2-8 harmonics can be expressed as:

$$x(n) = s(n) + q(n) \quad (18)$$

$$= A_m \exp(\varphi_m) \exp(j\omega_m n)$$

$$+ \sum_{h=2}^8 A_p \exp(j\omega_h n + \varphi_h) + q(n)$$

where  $A_h$  are shown in Table III [42], [43].  $\varphi_h$  is the initial phase which are selected at random in the range  $[0, 2\pi)$ . Due to the influence of harmonics, the overall estimation effect of our algorithm becomes less satisfactory as shown in Fig. 8.

*B. the case when the frequency, the amplitude and the phase all step change*

Let's consider the case when the frequency, the amplitude and the phase all step change when  $U_1 = 0.9 \exp(10\pi/180)$  and  $U_2 = \exp(80\pi/180)$ . Set  $l_1 = l_2 + 0.5$ . As shown in Fig. 9, our method achieve the minimum MSE -75dB when  $L=64$  and  $SNR=40$ dB. Fig. 10 illustrates that the MSEs of our

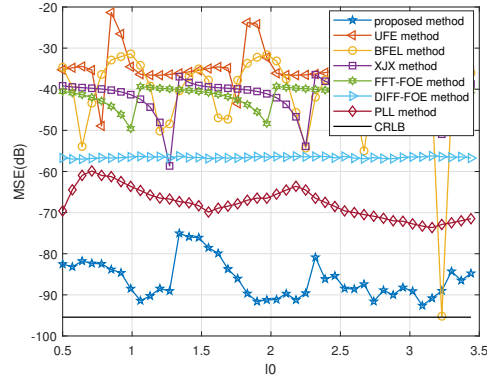


Fig. 8: MSEs of  $\hat{\omega}_0$  versus  $l_0$  distorted by 2-7 harmonics with  $SNR=40$ dB and  $L=32$

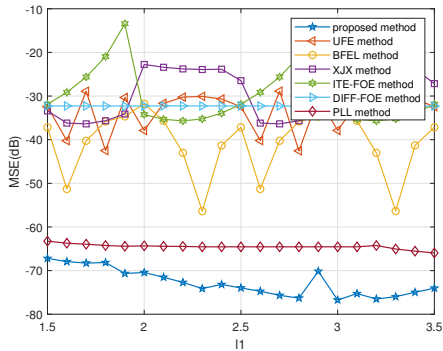
method decrease linearly when  $SNR$  increases, which means only our methods can estimate the frequency accurately with a step change in the frequency of the signal. As shown in Fig. 11, when  $40 < L < N - 3$ , our method can estimate  $l_1$  accurately. When  $2 < L < 80$ , our method can estimate  $l_2$  accurately. Besides, our method achieves the minimum MSE -75dB when  $L=64$  is in the interval  $[50, 100]$ . Therefore, our method has a better performance when  $L$  is in the interval  $[3, N-4]$  in the case that the frequency step change. The reason for  $L$  taking this interval is as follows. In our algorithm, the signal sequence with step-changed frequency is equivalent to a signal sequence formed by splicing two single-frequency complex exponential signals with different frequencies. For single-frequency complex exponential signals, at least two consecutive samples of  $s(n)$  and  $s(n+1)$  can accurately estimate the corresponding frequency. In other words, for a single-frequency complex exponential signal, at least two samples are required to fully describe it. Our algorithm considers two single-frequency complex exponential signals jointly. Simulation shows that for each single-frequency complex exponential signal, at least three consecutive samples are required to fully describe its complete information. Therefore, the variation range of  $L$  is actually  $[3, N - 4]$ . When  $L < 3$ , the frequency of  $\omega_1$  cannot be estimated; when  $L > N - 4$ , the frequency of  $\omega_2$  cannot be estimated.

In order to verify the effect of different sampling points  $N$  on the estimated frequency, Set  $l_1=1.5$ ,  $l_2=0.5$  and  $SNR=40$ dB. The MSE of frequency is shown in Table IV, and the results show that our method has better effect under different sampling points  $N$  when  $L = \frac{N}{2}$ .

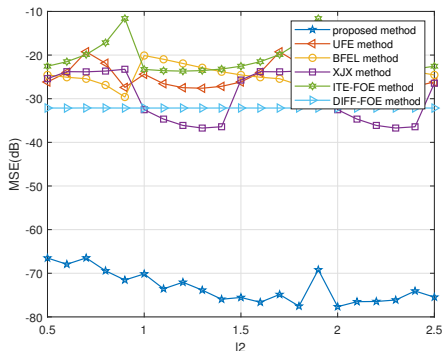
The signal distorted by the DC offset is shown in Fig. 12

TABLE IV: MSEs of  $\hat{\omega}_1$  and  $\hat{\omega}_2$  with different sampling points  $N$  when  $L = \frac{N}{2}$  and SNR = 40dB(unit: dB)

	Proposed Method	UFE Method	BFEL Method	XJX Method	ITE-DFT Method	DIFF-DFT Method	PLL Method
N=128	$l_1$	-72.54	-49.51	-54.64	-29.56	-14.93	-34.65
	$l_2$	-70.04	-26.28	-26.00	-23.33	-16.79	-
N=256	$l_1$	-81.68	-54.04	-60.21	-35.63	-21.19	-40.70
	$l_2$	-80.39	-32.40	-32.04	-29.37	-23.13	-41.71
N=512	$l_1$	-90.63	-59.33	-65.94	-41.67	-27.34	-46.74
	$l_2$	-89.29	-38.43	-38.0	-35.40	-29.33	-47.67
N=1024	$l_1$	-98.73	-65.08	-71.84	-47.70	-33.43	-52.74
	$l_2$	-98.93	-44.48	-44.05	-41.43	-35.43	-53.70

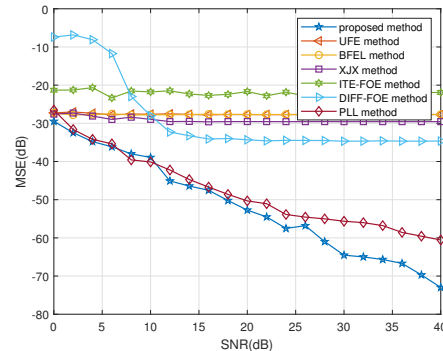


(a)

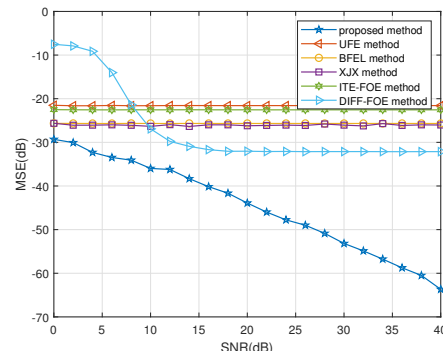


(b)

Fig. 9: The relationships between  $l_i$  ( $i = 1, 2$ ) and MSEs of  $\hat{\omega}_1$  and  $\hat{\omega}_2$  when SNR=40dB and  $L = 64$  (a)  $l_1$ ; (b)  $l_2$



(a)



(b)

Fig. 10: The relationships between SNR and MSEs of  $\hat{\omega}_1$  and  $\hat{\omega}_2$  when  $l_1 = 1.5$ ,  $l_2 = 0.5$  and  $L = 64$  (a)  $l_1$ ; (b)  $l_2$

and the signal distorted by the harmonics of part A is shown in Fig. 13.

### C. Computational Complexity

We give the computational complexity analysis of our method. As shown in Eq. (12), three different DFT bins  $X(k)$  are needed to establish the equation for the amplitude or phase jump signal. The evaluation of one DFT sample requires  $N$  complex multiplications and  $N-1$  complex additions. To compute the frequency parameters, we need a  $3 \times 3$  complex matrix inverse operation. If the Gauss elimination method is used, the evaluation of  $6 \times 6$  matrix inversion requires  $\sum_{p=1}^6 p \times p$  complex multiplications and  $\sum_{p=0}^5 p \times p$  complex additions. Therefore, the

overall complexity of the proposal is  $PN + \sum_{p=1}^P p \times p$  complex

multiplications and  $P(N-1) + \sum_{p=0}^{P-1} p \times p$  complex additions.

$P=5$  for the case when the frequency step changes and  $P=3$  for the case when the amplitude and the phase both step change.

## IV. PMU TEST

In the power systems, we select 50.5 Hz as the reference frequency, 5800 Hz as the sampling frequency and the length of the signal sequence is 128 and the specific frequency is denoted as  $f_i$  ( $i = 0, 1, 2$ ). Eq. (1) is often used to describe the balanced three-phase voltage signal by means of the Clark transform [51]. In power system, the step changes of amplitude, phase and frequency are the three important conditions which should be considered. Therefore, the basis of

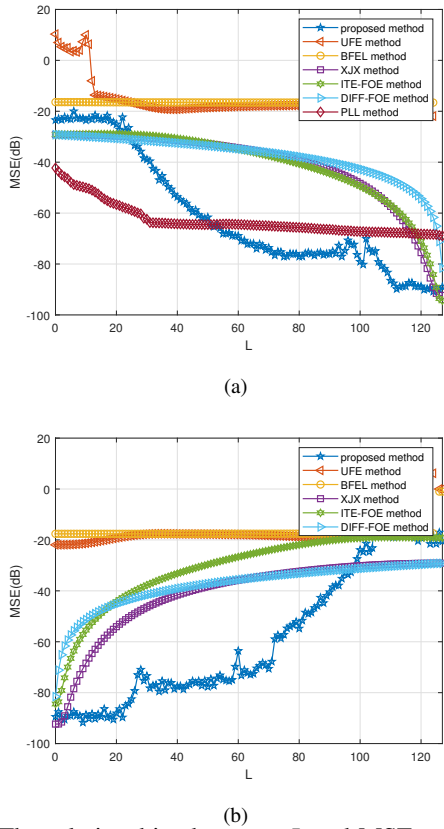


Fig. 11: The relationships between  $L$  and MSEs of  $\hat{\omega}_1$  and  $\hat{\omega}_2$  when  $l_1 = 1.5$ ,  $l_2 = 0.5$  and SNR=40dB (a)  $l_1$ ; (b)  $l_2$

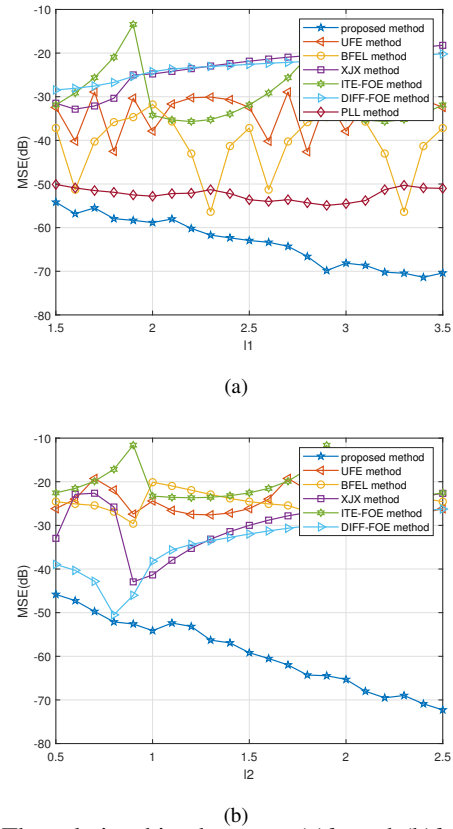


Fig. 12: The relationships between (a)  $l_1$  and (b)  $l_2$  and MSEs of  $\hat{\omega}_1$  and  $\hat{\omega}_2$  with SNR=40dB,  $A_{dc} = 1$  and  $L=64$

375 the power quality assessment is a fast and accurate frequency  
 376 estimation method under an abrupt signal step. To evaluate the  
 377 dynamic response when exposed to an abrupt signal change,  
 378 a positive step followed by a reverse step back to the starting  
 379 value under various conditions is applied to the amplitude,  
 380 phase angle, and frequency of the signal, respectively.

#### 381 A. Results Under the Parameters Step Signal Condition

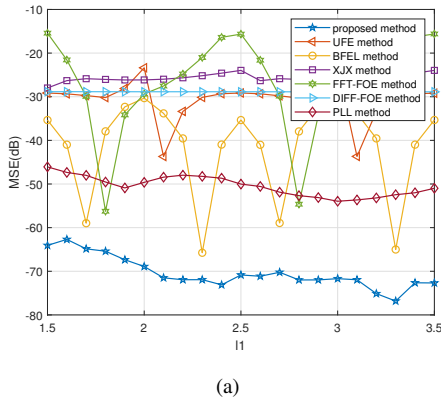
382 Firstly, let's consider the case when the amplitude and the  
 383 phase step change, and the frequency keeps unchanged. Fig.  
 384 14 and Fig. 15 show the results of simulation for step change  
 385 signals in the magnitude and the phase with SNR=40dB. The  
 386 magnitude step size is set to 0.1, and the phase step size is  
 387 set to  $\pi/18$ . Step changes occur at  $t = 0.15$  sec and are  
 388 released at  $t = 0.3$  sec. The proposed algorithm follows the  
 389 reference frequency even when the step change occurs and is  
 390 released. The PLL algorithm can also estimate the frequency  
 391 well under the condition that the frequency keeps constant.  
 392 The simulation results of Fig. 14 and Fig. 15 show that the  
 393 MSE of the PLL algorithm can reach -76.56dB and -79.78dB,  
 394 respectively. Our algorithm mse can roughly reach -95.18dB  
 395 and -98.05dB before and after the step change. However, the  
 396 UFE algorithm can accurately estimate  $\omega_0$  for step change  
 397 signals in the magnitude or the phase only when the jump  
 398 point  $L$  is in the interval [44,86].

399 Fig. 16 and Fig. 17 show the performances of our method  
 400 for the signal with step-changed frequency in the noiseless or

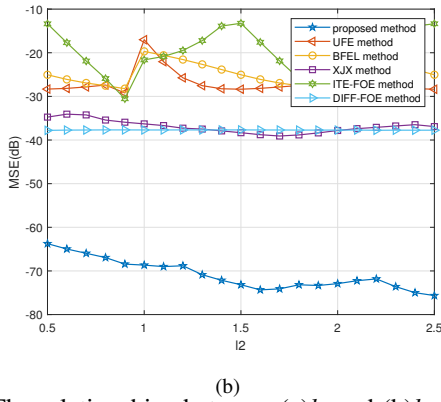
noisy environment. The dynamic response of our algorithm  
 needs to be discussed respectively. The reference frequency  
 50.5 Hz changes to 60.5 Hz at  $t = 1$  sec and is released at  
 $t = 2$  sec. When the jump point  $L < 88$ , our algorithm can  
 accurately estimate  $\omega_1$ . When the jump point  $L > 40$ , our  
 algorithm can accurately estimate  $\omega_2$ . When the jump point  
 $L$  is in the interval  $L \in [41, 88]$ , our algorithm can accurately  
 estimate  $\omega_1$  and  $\omega_2$  at the same time.

For the  $N$ -sample signal with the step-changed magnitude  
 and phase, the total length of signal with the angular frequency  
 $\omega_0$  keeps the length of  $N$  unchanged. The information of the  
 angular frequency  $\omega_0$  always exists in the  $N$  sampling points.  
 Therefore, when  $L$  is the interval  $[0, N - 1]$ , as shown in  
 Fig. 14 and Fig. 16, the estimation accuracy of the algorithm  
 remains unchanged. For the  $N$ -sample signal with the step-  
 changed frequency, the information of  $\omega_1$  only contains the  
 first  $L$  sampling points and the information of  $\omega_2$  only contains  
 the last  $N - L$  sampling points. For the signal with length  $N$ ,  
 with the increase of the  $L$ , the influence of  $\omega_1$  in observation  
 sequence is greater, and the anti-noise perform of  $\omega_1$  is better.  
 The smaller  $L$  is, the greater the influence of  $\omega_2$  in observation  
 sequence is, and the better the anti-noise perform  $\omega_2$  is.  
 Therefore, as shown in Fig. 16, the estimated performance  
 of  $\omega_1$  will be improved with the increase of  $L$ . The estimated  
 performance of  $\omega_2$  will be improved with the decrease of  $L$ .  
 The sampling frequency is set to 1800 Hz. In our method,  
 rise time occurs when  $t = 1.0011s$  ( $L = 126$ ), peak time





(a)



(b)

Fig. 13: The relationships between (a)  $l_1$  and (b)  $l_2$  distorted by 2-7 harmonics and MSEs of  $\hat{\omega}_1$  and  $\hat{\omega}_2$  with SNR=40dB and  $L=64$

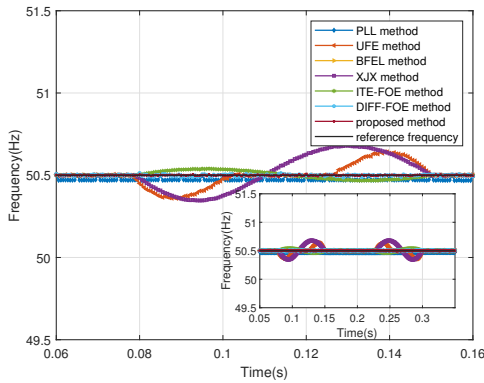


Fig. 14: The estimated frequencies of simulation for step change signals in the magnitude when SNR=40dB.

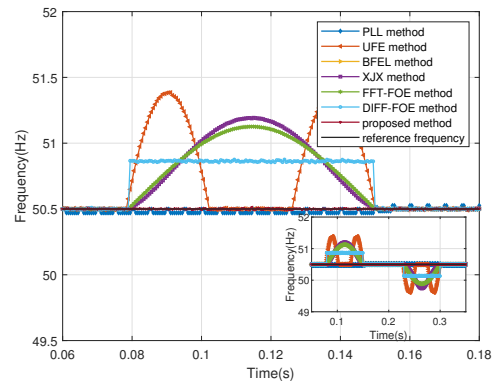


Fig. 15: The estimated frequencies of simulation for step change signals in the phase when SNR=40dB.

value.

It can be observed from Fig. 17 that the minimum MSE of  $\omega_1$  and  $\omega_2$  can reach -122.58dB and -161.51dB when  $L = 3$  in the noiseless environment respectively. Within the allowable error range, there is neither overshoot nor undershoot. When the sampling frequency is set to  $f_s$ , the rise time, peak time and adjustment time are all  $3/f_s$ . To sum up, the PLL can quickly achieve frequency tracking of the step signal in the noisy environment. However, our method has a larger maximum error in the noisy environment. However, it has a considerable advantage that the angular frequencies  $\omega_1$  and  $\omega_2$  before and after the frequency step change can be calculated simultaneously.

436  
437  
438  
439  
440  
441  
442  
443  
444  
445  
446  
447  
448

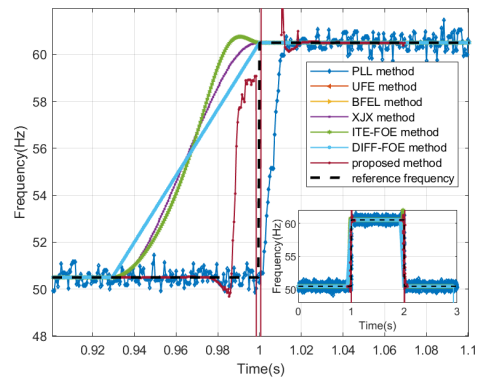


Fig. 16: The estimated frequencies of simulation for step change signals in the frequency when SNR=40dB.

### B. Results Under IEEE C37.118.-2014 Standard

This section presents the simulation results of P-Class and M-Class synchrophasor measurements for the power system with 50.5 Hz signal frequency. According to IEEE C37.118.-2014 standard, the estimated performances of various algorithms are compared with an amplitude modulated signal, a phase modulated signal and a ramp signal. Eq. (20) gives the

449  
450  
451  
452  
453  
454  
455

occurs when  $t = 1.0089s$  ( $L = 112$ ), and adjustment time occurs when  $t = 1.0221s$  ( $L = 88$ ). The overshoot has reached 79.2% according to Eq. (18). For the PLL method, rise time occurs when  $t = 1.0094s$  ( $L = 111$ ). Peak time occurs when  $t = 1.0128s$  ( $L = 105$ ) respectively. The overshoot has reached 9.4%.

$$\frac{X_{\max} - X(\infty)}{X(\infty)} \times 100\% \quad (19)$$

where  $X_{\max}$  represents the instantaneous maximum deviation of the adjustment value, and  $X(\infty)$  represents the steady-state

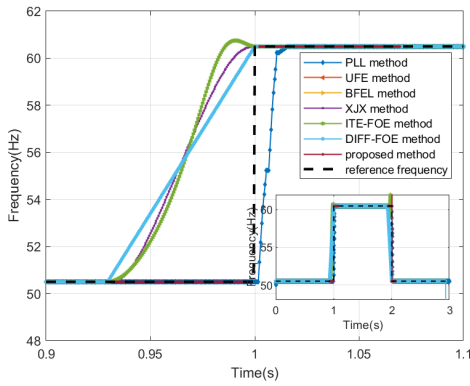


Fig. 17: The estimated frequencies of simulation for step change signals in the frequency under noiseless conditions.

456 amplitude modulated and phase modulated signal and Eq. (21)  
457 gives the chirp signal.

$$X_1 = A [1 + \alpha \cos(2\pi f_1 t)] \times \cos [2\pi f_0 t + \beta \cos(2\pi f_1 t - \pi)] \quad (20)$$

$$X_2 = A_1 e^{j(2\pi f_1 t + \pi R_f t^2)} \quad (21)$$

458 The frequency error ( $|FE|$ ), the total vector error (TVE) and  
459 rate of change of frequency (ROCOF) are used as the index  
460 to evaluate the performance of the considered methods.  $|FE|$ ,  
461 TVE and ROCOF are defined as follows:

$$|FE| = |\hat{f} - f| \quad (22)$$

$$TVE = \sqrt{\frac{(\hat{A}_r - A_r)^2 + ((\hat{A}_i - A_i))^2}{(A_r)^2 + (A_i)^2}} \times 100\% \quad (23)$$

$$ROCOF = \frac{\hat{f}(n) - \hat{f}(n-1)}{T_{RR}} \quad (24)$$

462 where  $\hat{A}_r$  and  $\hat{A}_i$  are the real and imaginary parts of the  
463 estimated amplitude,  $A_r$  and  $A_i$  are the real and imaginary  
464 parts of the true amplitude,  $\hat{f}$  is the estimated frequency and  
465  $f$  is the true frequency of the signal.  $T_{RR} = 1/f_{RR}$  and  $f_{RR}$  is  
466 the PMU reporting rate.

467 We will divide this part of simulation into two parts ac-  
468 cording to section III. The initial parameters are all set as  $N$   
469  $= 128$  and  $f_s = 6400$  Hz. The average values and max values  
470 of  $|FE|$ , TVE and ROCOF of all the considered methods will  
471 be shown in the following six tables.

472 1) *Amplitude modulation signal*: In the first case when the  
473 amplitude and the phase step change when the frequency keeps  
474 unchanged,  $\beta$  is set to 0.  $\alpha$  is set to -0.1 and 0.1 respectively  
475 before and after the step change. 0.2 per unit amplitude  
476 variation with 1.0 Hz of frequency is applied to the single-  
477 stone signal and the system frequency is set to 50.5 Hz. The  
478 average values of  $|FE|$ , TVE and ROCOF of all the compared  
479 methods are shown in Table V-VII. In the second case when  
480 the frequency, the amplitude and the phase all step change, the  
481 frequency is set to 50.5 Hz and 20.8 Hz respectively before and  
482 after the step change. Other parameters remain unchanged in  
483 the first case. The estimated results are shown in Table VIII-X.

2) *Phase modulation signal*: In the first case when the  
484 amplitude and the phase step change,  $\alpha$  is set to 0.  $\beta$  is set  
485 to -0.1 and 0.1 respectively before and after the step change.  
486 Modulation frequency and system frequency are referred to the  
487 amplitude modulated signal shown above. The average values  
488 of  $|FE|$ , TVE and ROCOF of all the compared methods are  
489 shown in Table V-VII. In the second case when the frequency,  
490 the amplitude and the phase all step change and the frequency  
491 is set to 50.5 Hz and 20.8 Hz respectively before and after the  
492 step change. Other parameters remain unchanged in the first  
493 case. The estimated results are shown in Table VIII-X.

3) *Ramp signal*: In the first case when the amplitude and  
495 the phase step change, the positive ramp rate is 1.0 Hz/sec  
496 and the negative ramp rate is -1.0 Hz/sec. The amplitude  
497 before and after the step change is set to 1 and 0.9 respectively.  
498 The estimated results are shown in Table V-VII. In the second  
499 case when the frequency, the amplitude and the phase all step  
500 change, and the frequency is set to 50.5 Hz and 20.8 Hz  
501 respectively before and after the step change. Other parameters  
502 remain unchanged in the first case. The estimated results are  
503 shown in Table VIII-X.

## V. EXPERIMENTAL VERIFICATION

506 In this section, we will demonstrate the advantages of our  
507 method in actual conditions. Eq. (1) can be used to describe the  
508 modulation signals in the wireless systems, such as quadrature  
509 amplitude modulation signal (QAM), phase-shift keying signal  
510 (PSK) and frequency-shift keying signal (FSK) [40], [41].  
511 QAM signal, PSK signal and FSK signal are the most widely  
512 used modulation modes in communication.

513 We select the WLAN RF conformance testing, which is  
514 the most conformed one in the field of IM. The WLAN RF  
515 conformance testing has been widely used in the practical  
516 application. The channel environment in the WLAN RF con-  
517 formance testing is simple and idealized. Most interferences  
518 in the actual wireless communication can be ignored during  
519 the testing. Engineers of the RF conformance testing choose  
520 the method in Ref. [50], which is also compared in this paper,  
521 to estimate the carrier frequency offset(COF).

522 “NI WLAN Analysis” is a wireless RF conformance test  
523 system developed by National Instruments [52]. This test  
524 system provides the functions of signal generation and analysis  
525 for the test application of WLAN 802.11a/b/g/j/p/n/ac/ax/be.  
526 One of the most important functions of this test system is  
527 to judge whether the test results of the DUT(device under  
528 test) meet the test standard. A typical SISO test platform is  
529 shown in Fig. 18. Part ③ is the DUT, which is a wireless  
530 router supporting 802.11 ax. The output interfaces of the  
531 DUT is connected directly to the input interfaces of the RF  
532 conformance tester through a green specific cables, which  
533 is the part ④ in Fig. 18. The MIMO test scenario can be  
534 regarded as several SISO testers working in parallel. Keeping  
535 the physical connection form between the DUT and the tester  
536 unchanged, we can assemble a MIMO system with several  
537 same SISO systems. As the test system should be placed in  
538 a microwave anechoic chamber to avoid noise interference,  
539 the communication model in the RF test system is simple

TABLE V: Average |FE| (Hz) of all comparative methods

	Proposed	UFE	BFEL	XJX	ITE-DFT	DIFF-DFT	PLL
Off-nominal frequencies	0.016	0.512	19.189	0.256	0.189	0.053	0.021
Harmonic distortions	0.215	10.806	8.539	6.958	6.235	5.322	0.256
Amplitude modulation	0.015	1.074	20.310	0.548	0.307	0.038	0.019
Phase modulation	0.026	1.798	19.222	1.028	1.009	0.840	0.030
Positive ramp	0.062	8.083	0.556	0.056	0.069	0.061	0.066
Negative ramp	0.062	0.052	0.629	0.071	0.058	0.061	0.065

TABLE VI: Average TVE(%) of all comparative methods

	Proposed	UFE	BFEL	XJX	ITE-DFT	DIFF-DFT	PLL
Off-nominal frequencies	0.783	4.420	24.861	3.974	2.543	1.179	0.831
Harmonic distortions	0.059	0.165	0.062	0.212	0.145	0.197	0.064
Amplitude modulation	0.105	4.863	20.093	4.316	2.249	0.324	0.167
Phase modulation	0.074	12.714	82.722	10.064	9.855	8.061	0.079
Positive ramp	0.004	0.010	0.004	0.096	0.026	0.013	0.009
Negative ramp	0.006	0.129	0.844	0.038	0.020	0.011	0.011

TABLE VII: ROCOF estimator

	Proposed	UFE	BFEL	XJX	ITE-DFT	DIFF-DFT	PLL
Amplitude modulation	0.003	0.008	0.003	0.002	0.010	0.010	0.005
Phase modulation	0.003	0.011	0.002	0.003	0.002	0.009	0.005
Positive ramp	0.004	0.010	0.005	0.004	0.002	0.013	0.006
Negative ramp	0.004	0.008	0.004	0.003	0.002	0.013	0.006

540 and idealistic, where the specific cable is used to connect the  
 541 communication link. Testers do not need to consider the signal  
 542 attenuation and distortion caused by various interferences in  
 543 actual wireless communication, such as multipath effects.

544 “NI WLAN Analysis Soft Front Panel” is shown in Fig. 19.  
 545 With the zero-IF technique, 2.4G Hz WLAN signal is received  
 546 and down converted to baseband signal. After synchroniza-  
 547 tion, the I/Q measurement, carrier frequency estimation and  
 548 demodulation, the tester calculates the EVM (Error Vector  
 549 Magnitude) to evaluate the RF performances of DUT. As  
 550 shown in Fig.19, the COF is an important index in RF  
 551 conformance test. According to the test requirement, the tester  
 552 needs to measure the frequency offset of each subcarrier.  
 553 Under this test requirement, only the subcarrier to be tested is  
 554 allowed to transmit signals, and the remaining subcarriers are  
 555 prohibited from transmitting signal. The tester can control the  
 556 DUT to complete the above functions with the AT command.

In summary, the communication model in the RF test system  
 is simple and idealistic. The state-of-the-art methods, which  
 can be used in the high-speed digital communication networks,  
 are not needed to the algorithm engineers of RF conformance  
 testing. On the contrary, although they aren’t applicable for  
 the actual wireless communication, the methods in Refs. [49],  
 [50] and our method are suitable for the RF conformance  
 testing. Let’s take 802.11 ax as an example. The transmission  
 power and the receiving power used in “NI WLAN Analysis”  
 are 10dBm and 20dBm. The line loss is about 3dBm. Then  
 bandwidth of 802.11 ax signal is 20 MHz. The sampling fre-  
 quency is set  $f_s = 1.25 \cdot \text{bandwidth} = 25\text{MHz}$ . With the zero-IF  
 technique, the 2.4G Hz 802.11ax signal is received and down  
 converted to baseband signal. Without the carrier frequency  
 offset, the frequency points of subcarriers in baseband are 0Hz,  
 20/K Hz, 40M/K Hz....., where K is the total number of  
 subcarriers. When frequency offset exists, the frequency point

TABLE VIII: Average |FE| (Hz) of all comparative methods

		Proposed	UFE	BFEL	XJX	ITE-FOE	DIFF-FOE	PLL
Off-nominal frequencies	$\omega_1$	0.182	18.972	19.995	9.656	35.404	8.853	0.235
	$\omega_2$	0.268	25.214	24.191	39.343	65.091	20.834	-
Harmonic distortions	$\omega_1$	1.082	18.167	18.976	17.047	19.062	2.232	1.131
	$\omega_2$	2.232	22.386	22.243	26.322	28.546	24.327	-
Amplitude modulation	$\omega_1$	0.006	3.103	2.781	3.900	2.728	3.528	0.011
	$\omega_2$	0.003	4.083	3.405	0.588	1.415	1.159	-
Phase modulation	$\omega_1$	0.016	3.860	2.101	3.838	2.534	3.919	0.021
	$\omega_2$	0.011	3.326	4.086	6.526	6.222	5.768	-
Positive ramp	$\omega_1$	0.031	0.251	0.261	0.199	0.426	0.106	0.036
	$\omega_2$	0.031	0.598	0.423	0.440	0.728	0.354	-
Negative ramp	$\omega_1$	0.031	0.293	0.259	0.189	0.254	0.168	0.036
	$\omega_2$	0.032	0.575	0.425	0.386	0.540	0.292	-

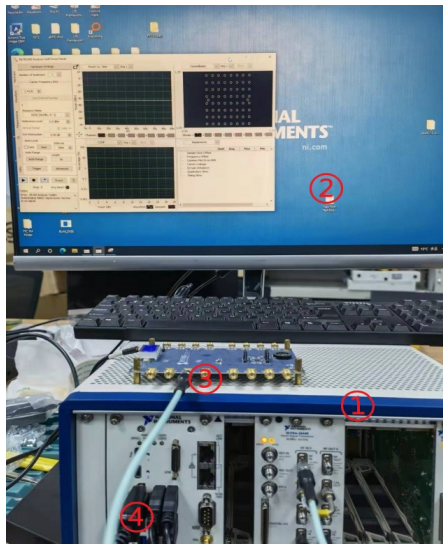


Fig. 18: The test system ①test platform device; ②screen; ③the DUT(device under test); ④the input interfaces through cables.

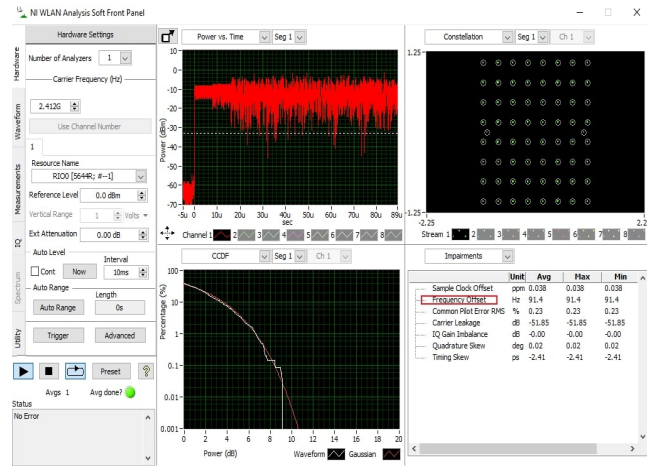


Fig. 19: NI WLAN Analysis Soft Front Panel.

574 of  $k$ -th subcarrier is  $\Delta f_k + k \frac{20}{K}$  MHz, where  $\Delta f_k$  is the frequency  
 575 offset and its value is no more than 100Hz. We select the  
 576 0-th subcarrier as the research object and set the frequency  
 577 offset as 91.4Hz. The 64-QAM signals are sent by the DUT  
 578 and measured by “NI WLAN Analysis”. We cooperate with  
 579 algorithm engineers of NI to give a performance comparison  
 580 in the case that the two adjacent symbols jump, when  $N$   
 581 = 128 and  $L = 64$ . The comparison results are shown in  
 582 Table XI. Our method can accurately estimate the frequency  
 583 in the two-symbol combination scenario. When the difference  
 584 between the two symbols is large (such as  $U_1 = 1 + j$  and

$U_1 = 1 + 7j$ ), the method proposed in [50] can still estimate  
 the actual carrier. In addition, if we select the first 64 sample  
 points of the signal, the signal is a single carrier signal with  
 the constant amplitude, frequency and phase. At this time,  
 the carrier can be accurately estimated by Refs. [49], [50].  
 The MSEs of the two algorithms in noise-free are -312dB  
 and -337dB. The MSEs of the two algorithms in “NI WLAN  
 Analysis” are -87dB and -85dB. Therefore, in the noisy state,  
 if we select the 64-point sampling point corresponding to a  
 symbol for the estimation in Refs. [49], [50], the estimation  
 results are respectively close to and slightly worse than the  
 estimation result obtained by our algorithm with 128 adjacent  
 sampling points of two different symbols.

TABLE IX: Average TVE(%) of all comparative methods

		Proposed	UFE	BFEL	XJX	ITE-FOE	DIFF-FOE	PLL
Off-nominal frequencies	$\omega_1$	0.313	12.225	10.102	19.697	28.236	17.040	0.358
	$\omega_2$	0.155	1.082	0.502	0.609	5.366	0.757	-
Harmonic distortions	$\omega_1$	2.531	14.057	11.203	18.011	21.272	12.599	2.582
	$\omega_2$	2.543	14.172	13.543	19.432	24.212	13.122	-
Amplitude modulation	$\omega_1$	0.116	12.077	10.000	21.449	17.429	19.048	0.162
	$\omega_2$	0.078	35.462	7.456	46.934	16.657	22.939	-
Phase modulation	$\omega_1$	1.224	16.028	10.000	19.072	19.848	21.520	1.269
	$\omega_2$	1.843	16.553	19.037	31.641	22.159	25.062	-
Positive ramp	$\omega_1$	0.010	1.240	0.830	0.337	5.369	0.567	0.015
	$\omega_2$	0.154	1.082	0.502	0.609	5.366	0.756	-
Negative ramp	$\omega_1$	0.350	1.687	0.884	0.475	0.467	0.837	0.403
	$\omega_2$	0.991	1.418	0.600	0.749	0.715	0.635	-

TABLE X: ROCOF estimator

		Proposed	UFE	BFEL	XJX	ITE-FOE	DIFF-FOE	PLL
Amplitude modulation	$\omega_1$	0.001	0.004	0.001	0.002	0.003	0.010	0.005
	$\omega_2$	0.001	0.004	0.001	0.002	0.003	0.010	-
Phase modulation	$\omega_1$	0.020	0.006	0.002	0.004	0.048	0.009	0.025
	$\omega_2$	0.246	23.326	23.086	40.526	79.222	15.768	-
Positive ramp	$\omega_1$	0.043	19.579	4.201	25.795	55.027	0.016	0.048
	$\omega_2$	0.637	19.580	4.201	25.795	55.027	0.016	-
Negative ramp	$\omega_1$	0.086	22.696	4.117	24.382	32.778	0.016	0.091
	$\omega_2$	0.635	22.697	4.117	24.382	32.779	0.016	-



TABLE XI: MSEs of  $\hat{\omega}_0$  with different combinations of 64QAM symbol (unit: dB)

	Proposed Method	UFE Method	BFEL Method	XJX Method	ITE-DFT Method	DIFF-DFT Method	PLL Method
{1 + j, 1 + 3j}	-98.9064	-90.6185	-41.8568	-28.6852	-36.5555	-75.7581	-96.4532
{1 + j, 1 + 5j}	-99.2897	-95.1879	-33.8279	-28.6842	-34.3535	-90.5598	-96.9367
{1 + j, 1 + 7j}	-100.0315	-96.9839	-26.2352	-28.6839	-33.5013	-96.5699	-96.4578
{1 + j, -1 - j}	-94.9775	-93.7092	-41.4395	-30.0236	-33.4679	-76.3738	-94.7346
{1 + j, -1 - 3j}	-98.6781	-97.5644	-28.8736	-29.5114	-32.8817	-77.8916	-95.3346
{1 + j, -1 - 5j}	-96.2039	-95.8673	-31.3567	-28.0228	-27.5122	-91.1075	-96.0328
{1 + j, -1 - 7j}	-99.7640	-99.6668	-23.8708	-29.2829	-32.5654	-94.2626	-96.7843

VI. CONCLUSION

The IpDFT algorithm proposed in this paper effectively estimates the frequency of the single tone signal with parameter step change in the sampling signal sequence. The relationship between the DFT bins and the step changed parameters is given by several linear equations. At most six different DFT bins are used to eliminate the effect of the parameter (frequency, amplitude or phase) step change on the  $L$ -th sample. The results of simulation and experiment confirm that the proposed algorithm gives precise results. As a future work, we will study an improved method for the multi-frequency signal with multi-symbol step change.

REFERENCES

[1] Z. Oubrahim, V. Choqueuse, Y. Amirat, and M. E. H. Benbouzid, "Maximum-likelihood frequency and phasor estimations for electric power grid monitoring," *IEEE Trans. Ind. Informat.*, vol. 14, no. 1, pp. 167–177, 2018.

[2] V. Choqueuse, A. Belouchrani, F. Auger, and M. Benbouzid, "Frequency and phasor estimations in three-phase systems: Maximum likelihood algorithms and theoretical performance," *IEEE Trans. Smart Grid*, vol. 10, no. 3, pp. 3248–3258, 2019.

[3] K. Chauhan, M. V. Reddy, and R. Sodhi, "A novel distribution-level phasor estimation algorithm using empirical wavelet transform," *IEEE Trans. Ind. Electron.*, vol. 65, no. 10, pp. 7984–7995, 2018.

[4] S. Reza, M. Ciobotaru, and V. G. Agelidis, "Accurate estimation of single-phase grid voltage fundamental amplitude and frequency by using a frequency adaptive linear kalman filter," *IEEE J. Emerg. Sel. Top. Power Electron.*, vol. 4, no. 4, pp. 1226–1235, 2016.

[5] H. Ahmed, S. Biricik, and M. Benbouzid, "Linear kalman filter-based grid synchronization technique: An alternative implementation," *IEEE Trans. Ind. Informat.*, pp. 1–1, 2020.

[6] H. Ahmed, S. Amamra, and I. Salgado, "Fast estimation of phase and frequency for single-phase grid signal," *IEEE Trans. Ind. Electron.*, vol. 66, no. 8, pp. 6408–6411, 2019.

[7] S. Nam, S. Kang, L. Jing, and S. Kang, "A novel method based on prony analysis for fundamental frequency estimation in power systems," in *IEEE 2013 Tencon - Spring*, 2013, pp. 327–331.

[8] D. Belega, D. Fontanelli, and D. Petri, "Low-complexity least-squares dynamic synchrophasor estimation based on the discrete fourier transform," *IEEE Trans. Instrum. Meas.*, vol. 64, no. 12, pp. 3284–3296, 2015.

[9] D. Belega, D. Fontanelli, and D. Petri, "Dynamic phasor and frequency measurements by an improved taylor weighted least squares algorithm," *IEEE Trans. Instrum. Meas.*, vol. 64, no. 8, pp. 2165–2178, 2015.

[10] P. Romano and M. Paolone, "Enhanced interpolated-dft for synchrophasor estimation in fpgas: Theory, implementation, and validation of a pmu prototype," *IEEE Trans. Instrum. Meas.*, vol. 63, no. 12, pp. 2824–2836, 2014.

[11] A. Derviskadić, P. Romano, and M. Paolone, "Iterative-interpolated dft for synchrophasor estimation: A single algorithm for p- and m-class compliant pmus," *IEEE Trans. Instrum. Meas.*, vol. 67, no. 3, pp. 547–558, 2018.

[12] N. Nevaranta, S. Derammelaere, J. Parkkinen, and B. Vervisch, "Online identification of a mechanical system in frequency domain using sliding dft," *IEEE Trans. Ind. Electron.*, vol. 63, no. 9, pp. 5712–5723, 2016.

[13] X. Yang, J. Zhang, X. Xie, and X. Xiao, "Interpolated dft-based identification of sub-synchronous oscillation parameters using synchrophasor data," *IEEE Trans. Smart Grid*, vol. 11, no. 3, pp. 2662–2675, 2020.

[14] D. Belega, D. Macii, and D. Petri, "Fast synchrophasor estimation by means of frequency-domain and time-domain algorithms," *IEEE Trans. Instrum. Meas.*, vol. 63, no. 2, pp. 388–401, 2014.

[15] D. Macii, D. Petri, and A. Zorati, "Accuracy analysis and enhancement of dft-based synchrophasor estimators in off-nominal conditions," *IEEE Trans. Instrum. Meas.*, vol. 61, no. 10, pp. 2653–2664, 2012.

[16] E. Aboutanios and B. Mulgrew, "Iterative frequency estimation by interpolation on fourier coefficients," *IEEE Trans. Signal Process.*, vol. 53, no. 4, pp. 1237–1242, 2005.

[17] E. Aboutanios, "A modified dichotomous search frequency estimator," *IEEE Signal Process. Lett.*, vol. 11, no. 2, pp. 186–188, 2004.

[18] Y. Dun and G. Liu, "A fine-resolution frequency estimator in the odd-dft domain," *IEEE Signal Process. Lett.*, vol. 22, no. 12, pp. 2489–2493, 2015.

[19] H. Wen, C. Li, and L. Tang, "Novel three-point interpolation dft method for frequency measurement of sine-wave," *IEEE Trans. Ind. Informat.*, vol. 13, no. 5, pp. 2333–2338, 2017.

[20] H. Wen, J. Zhang, Z. Meng, and S. Guo, "Harmonic estimation using symmetrical interpolation fft based on triangular self-convolution window," *IEEE Trans. Ind. Informat.*, vol. 11, no. 1, pp. 16–26, 2015.

[21] J. Sun S. Ye and E. Aboutanios, "On the estimation of the parameters of a real sinusoid in noise," *IEEE Signal Process. Lett.*, vol. 24, 2017.

[22] Y. H. Kim, K. J. Son, S. Kang, and T. G. Chang, "Improved frequency estimation algorithm based on the compensation of the unbalance effect in power systems," *IEEE Trans. Instrum. Meas.*, pp. 1–1, 2020.

[23] T. Tyagi and P. Sumathi, "Frequency estimation based on moving-window dft with fractional bin-index for capacitance measurement," *IEEE Trans. Instrum. Meas.*, vol. 68, no. 7, pp. 2560–2569, 2019.

[24] A. Derviskadić, P. Romano, and M. Paolone, "Iterative-interpolated dft for synchrophasor estimation: A single algorithm for p- and m-class compliant pmus," *IEEE Trans. Instrum. Meas.*, vol. 67, no. 3, pp. 547–558, 2018.

[25] J. Zhang, L. Tang, A. Mingotti, L. Peretto, and H. Wen, "Analysis of white noise on power frequency estimation by dft-based frequency shifting and filtering algorithm," *IEEE Trans. Instrum. Meas.*, vol. 69, no. 7, pp. 4125–4133, 2020.

[26] D. Belega, D. Dallet, and D. Petri, "Accuracy of sine wave frequency estimation by multipoint interpolated dft approach," *IEEE Trans. Instrum. Meas.*, vol. 59, no. 11, pp. 2808–2815, 2010.

[27] D. Belega, D. Dallet, and D. Slepicka, "Accurate amplitude estimation of harmonic components of incoherently sampled signals in the frequency domain," *IEEE Trans. Instrum. Meas.*, vol. 59, no. 5, pp. 1158–1166, 2010.

[28] H. Wen, Z. Teng, and S. Guo, "Triangular self-convolution window with desirable sidelobe behaviors for harmonic analysis of power system," *IEEE Trans. Instrum. Meas.*, vol. 59, no. 3, pp. 543–552, 2010.

[29] D. Kania J. Borkowski and J. Mroczka, "Interpolated-dft-based fast and accurate frequency estimation for the control of power," *IEEE Trans. Ind. Electron.*, vol. 61, no. 12, pp. 7026–7034, 2014.

[30] J. Borkowski, J. Mroczka, A. Matusiak, and D. Kania, "Frequency estimation in interpolated discrete fourier transform with generalized maximum sidelobe decay windows for the control of power," *IEEE Trans. Ind. Inform.*, vol. 17, no. 3, pp. 1614–1624, 2021.

[31] Y. Sun, C. Zhuang, and Z. Xiong, "A scale factor-based interpolated dft for chatter frequency estimation," *IEEE Trans. Instrum. Meas.*, vol. 64, no. 10, pp. 2666–2678, 2015.

[32] Y. Sun, C. Zhuang, and Z. Xiong, "A switch-based interpolated dft for the small number of acquired sine wave cycles," *IEEE Trans. Instrum. Meas.*, vol. 65, no. 4, pp. 846–855, 2016.

- 715 [33] K. Wang, H. Wen, and G. Li, "Accurate frequency estimation by using  
716 three points interpolated dft based on rectangular window," *IEEE Trans.*  
717 *Ind. Informat.*, pp. 1–1, 2020.
- 718 [34] K. Wang, H. Wen, W. Tai, and G. Li, "Estimation of damping factor  
719 and signal frequency for damped sinusoidal signal by three points  
720 interpolated dft," *IEEE Signal Process. Lett.*, vol. 26, no. 12, pp. 1927–  
721 1930, 2019.
- 722 [35] K. Wang, H. Wen, L. Xu, and L. Wang, "Two points interpolated dft  
723 algorithm for accurate estimation of damping factor and frequency,"  
724 *IEEE Signal Process. Lett.*, vol. 28, pp. 499–502, 2021.
- 725 [36] K. Wang, L. Zhang, H. Wen, and L. Xu, "A sliding-window dft based  
726 algorithm for parameter estimation of multi-frequency signal," *Digit.*  
727 *Signal Prog.*, vol. 97, pp. 102617, 2019.
- 728 [37] S. Ando, "Frequency-domain prony method for autoregressive model  
729 identification and sinusoidal parameter estimation," *IEEE Trans. Signal*  
730 *Process.*, vol. 68, pp. 3461–3470, 2020.
- 731 [38] "IEEE 802, ieee p802.11ax/d0.4," 2016.
- 732 [39] "IEEE standard for information technology, part 11: Wireless lan  
733 medium access control (mac) and physical layer (phy) specifications," .
- 734 [40] Y. Liu, Y. Peng, S. Wang, and Z. Chen, "Improved fft-based frequency  
735 offset estimation algorithm for coherent optical systems," *IEEE Photon-*  
736 *ics Technol. Lett.*, vol. 26, no. 6, pp. 613–616, 2014.
- 737 [41] J. Han, W. Li, Z. Yuan, and Y. Zheng, "A simplified implementation  
738 method of  $m$  th-power for frequency offset estimation," *IEEE Photonics*  
739 *Technol. Lett.*, vol. 28, no. 12, pp. 1317–1320, 2016.
- 740 [42] "Ieee standard for synchrophasor measurements for power systems,"  
741 *IEEE Std C37.118.1-2011 (Revision of IEEE Std C37.118-2005)*, pp.  
742 1–61, 2011.
- 743 [43] "Ieee standard for synchrophasor measurements for power systems  
744 – amendment 1: Modification of selected performance requirements,"  
745 *IEEE Std C37.118.1a-2014 (Amendment to IEEE Std C37.118.1-2011)*,  
746 pp. 1–25, 2014.
- 747 [44] M. Karimi-Ghartemani, M. Mojiri, A. Safaee, and J. A. Walseth, "A new  
748 phase-locked loop system for three-phase applications," *IEEE Trans.*  
749 *Power Electron.*, vol. 28, no. 3, pp. 1208–1218, 2013.
- 750 [45] F. Baradarani, M. R. Dadash Zadeh, and M. A. Zamani, "A phase-  
751 angle estimation method for synchronization of grid-connected power-  
752 electronic converters," *IEEE Trans. Power Deliv.*, vol. 30, no. 2, pp.  
753 827–835, 2015.
- 754 [46] J. Ren and M. Kezunovic, "Real-time power system frequency and  
755 phasors estimation using recursive wavelet transform," *IEEE Trans.*  
756 *Power Deliv.*, vol. 26, no. 3, pp. 1392–1402, 2011.
- 757 [47] J. Xiao, J. Feng, J. Han, and W. Li, "Low complexity fft-based frequency  
758 offset estimation for m-qam coherent optical systems," *IEEE Photonics*  
759 *Technol. Lett.*, vol. 27, no. 13, pp. 1371–1374, 2015.
- 760 [48] A. Peng, G. Ou, and M. Shi, "Frequency estimation of single tone  
761 signals with bit transition," *IET Signal Process.*, vol. 8, pp. 1025–1031,  
762 2014.
- 763 [49] J. Han, W. Li, J. Xiao, and J. Feng, "Frequency offset estimation with  
764 multi-steps interpolation for coherent optical systems," *IEEE Photonics*  
765 *Technol. Lett.*, vol. 27, no. 19, pp. 2011–2014, 2015.
- 766 [50] J. Lu, Y. Tian, S. Fu, and X. Li, "Frequency offset estimation for 32-  
767 qam based on constellation rotation," *IEEE Photonics Technol. Lett.*,  
768 vol. 29, no. 23, pp. 2115–2118, 2017.
- 769 [51] Ž. Zečević, B. Krstajić, and T. Popović, "Improved frequency estimation  
770 in unbalanced three-phase power system using coupled orthogonal  
771 constant modulus algorithm," *IEEE Trans. Power Deliv.*, vol. 32, no.  
772 4, pp. 1809–1816, 2017.
- 773 [52] "<https://www.ni.com/zh-cn/shop/software/products/rfmx-wlan.html>," .